Available online at www.sciencedirect.com
SCIENCE DIRECT®
International Journal of Heat and Mass Transfer 48 (2005) 2508–2515
International Journal of HEAT and MASS TRANSFER
www.elsevier.com/locate/ijhmt

DeLIF measurement of pH distribution around dissolving CO_2 droplet in high pressure vessel

Satoshi Someya [a,*], Shigeru Bando [b], Yongchen Song [a], Baixin Chen [a], Masahiro Nishio [a]

[a] National Institute of Advanced Industrial Science and Technology, 1-2-1 Namiki, Tsukuba, Ibaraki 305-8564, Japan
[b] Department of Mechanical Engineering, University of Tokyo, 7-3-1 Hongo, Bunkyo-ku, Tokyo 113-8656, Japan

Received 13 February 2004; received in revised form 24 September 2004
Available online 16 March 2005

Abstract

It is established a precise DeLIF (Dual Emission Laser-Induced-Fluorescence) system for an instant measurement of pH field. This method is very important in studies of the biological impacts of CO_2 sequestration, i.e., effects of pH on organisms. Quinine and sulforhodamine were used as fluorescence dyes. The molar absorption coefficient and emission intensity of quinine depend on pH of aqueous solutions, while those of sulforhodamine are not affected by pH. The ratio of fluorescence intensities represents pH at each point of the image. As a result, the pH field was successfully measured with uncertainty of approximately ±0.005, for $3.0 < \text{pH}$.

Keywords: Carbon dioxide; Laser induced fluorescence; pH; Flow visualization

1. Introduction

Recently, particular attention of the world has been focused on global warming due to increased concentrations of carbon dioxide (CO_2) in the atmosphere. Alternative energy technology has been expected, however, mitigating the atmospheric CO_2 concentration is a pressing need. The sequestration of CO_2 into the ocean, first proposed by Marchetti [1], has been recognized as an effective and practical mitigation strategy. Geological CO_2 sequestration into aquifers is also an important approach.

Seawater and underground water is saline water. CO_2 solubility and the onset condition of hydrate formation are different in saline water from those found in pure water. The hydrate can be formed under certain conditions in both ocean and geological aquifer sequestration. In some options of the geological sequestration, temperature becomes higher than 304 K, and CO_2 changes its phase to be supercritical. Thus, the kind of solvent, the state of the interface between CO_2 and solvents seem to affect the characteristics of CO_2 dissolution.

A quantitative flow-visualization can help to understand the CO_2 dissolution behavior and to achieve the CO_2 sequestration with minimum environmental impacts and with public consensus. In addition, the quantitative and instant measurement technique may be able to alleviate the complications with estimating thermophysical properties about CO_2 dissolution.

* Corresponding author. Tel.: +81 29 861 7247; fax: +81 29 851 7523.
E-mail address: s.someya@aist.go.jp (S. Someya).

0017-9310/$ - see front matter © 2005 Elsevier Ltd. All rights reserved.
doi:10.1016/j.ijheatmasstransfer.2004.12.042

In a previous paper [2], we applied a single-color Laser Induced Fluorescence (LIF) method to investigate the dissolution behavior, using quinine and an ultraviolet laser light source. Quinine is a very good fluorescence indicator under lower pH conditions with a less quenching effect, however, the relatively unstable pulse of the laser light source decreases the reliability of measurement. Therefore, to ensure high accuracy and reliability, the Dual emission LIF (DeLIF) method [3–5] is applied in the present study.

2. Experimental setup

2.1. High-pressure vessel

The experimental apparatus is schematically shown in Figs. 1 and 2. The high-pressure vessel, of which volume capacity was about 30 cm^3, had three windows made of sapphire glass. The whole assembly was designed to withstand safely 15 MPa of pressure. The safety valve was set on, to work at 12 MPa. A pressure gauge worked with a range of 0–20 MPa and with an accuracy of ±0.3% of the measured value. An accumulator with nitrogen gas compensated any pressure fluctuations due to CO_2 dissolution and so on. The temperature was controlled by a regulator bath and measured by a Pt-100 resistance bulb thermometer with an accuracy of ±0.05 K.

The coolant flowed through a narrow gap area around the vessel covered with insulation material. A magneto-stirrer was used before experiments and kept inactive during experiments, to make the initial temperature uniform. In the present study as a confirmation of the DeLIF system, the temperature was set at 288 K, a condition in which CO_2 is not supercritical and cannot form the hydrate. The test cell was filled up with pure water until 6 MPa by a plunger pump. Then, water was pressurized using nitrogen gas until it reached the required initial pressure condition (9.81 MPa). After the temperature became stable at the required level, pressurized liquid CO_2 was injected from the top-side nozzle of 3.175 (1.5) mm in outer (inner) diameter. A CO_2 droplet was kept at the edge of the nozzle because the density of liquid CO_2 is lower than that of water under the pressure condition below 30 MPa.

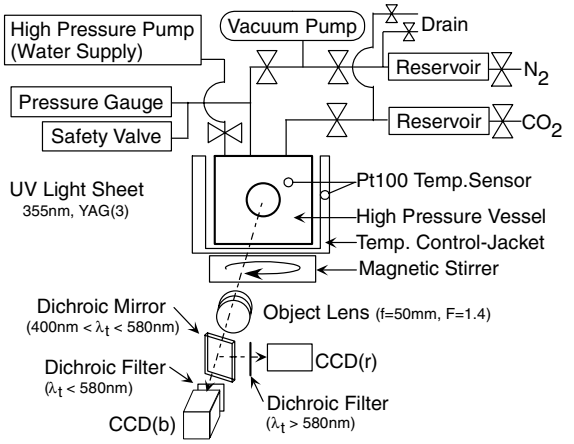

Fig. 1. Schematics of the experimental setup.

2.2. Measurement system

The optical system was composed of a light source and receiving parts as shown in Fig. 1. A third order harmonic of the Nd:YAG laser, wave length $\lambda =$

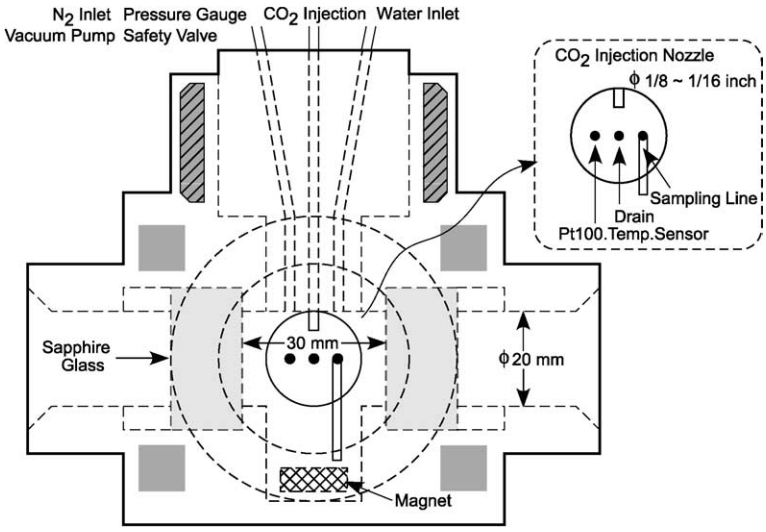

Fig. 2. Schematics of the high-pressure vessel.

355 nm, was used as the light source. The maximum frequency of the illumination pulse was 30 Hz and the output energy was 0.1–0.2 mJ/pulse. The light sheet was generated by cylindrical lenses and mirrors coated with multilayer films. The thickness of the light sheet was less than 0.5 mm. In the receiving optics, the fluorescence was collected by a lens ($f = 50$ mm, F1.4) and was split by a dichroic beam splitter, which transmitted wavelengths from 400 nm to 580 nm at an incident angle of 45°. The transmitted and reflected light was re-filtered by dichroic filters and was simultaneously recorded by each of 2 CCD cameras (8 bits, gray).

The position of each CCD camera was adjusted to capture the image of the nearly same spot, just below the CO_2 injection nozzle. The cameras did not require precise positioning because the physical and image coordinates were calibrated using a plate with an equally-spaced grid pattern at 0.5 mm intervals. The plate was fixed in the plane of the laser light sheet and images for the calibration were recorded at a pressure condition of 9.81 MPa. After finding the corresponding location between each grid point in the physical coordinates and those in the image coordinates, the image coordinate (X, Y) of the physical coordinate (x, y), which was expressed by the third order polynomial function of Eq. (1), was calculated by the least-square method as described by Sakakibara and Adrian [4]. This procedure compensated for the misalignment of cameras and the distortion due to refraction through the optical path of fluorescence from target to cameras.

$$X = \sum_{i=0}^{3}\sum_{j=0}^{3}\xi_{ij}x^i y^j, \quad Y = \sum_{i=0}^{3}\sum_{j=0}^{3}\eta_{ij}x^i y^j$$
$$\zeta_{ij} = \eta_{ij} = 0 \text{ for } (i+j>3) \tag{1}$$

2.3. Selection of dyes and spectral characteristics

If the intensity of the excitation light and the concentration of dye can be kept constant, the single-color LIF is applicable to measure the pH distribution. The intensity, however, is unstable in the case of a pulse-laser. The influence of the fluctuating intensity of excitation light can be cancelled out by applying the DeLIF technique, which uses two kinds of fluorescence dye.

In the case of a pH-dependent dye such as quinine, the molar absorptivity, ε, depends on pH and the fluorescence intensity at each point, $I(\mathrm{pH})$, is expressed by Eq. (2), where I_0 is the excitation intensity, C is the molar concentration of dye, φ is the quantum efficiency, L is the length of the sampling region along the path of the incident light, F is a fraction of the light coming into the camera.

$$I(\mathrm{pH}) = I_0 \mathrm{e}^{-\varepsilon(\mathrm{pH})LC}\varphi\varepsilon(\mathrm{pH})CF \tag{2}$$

The relation between the molar absorption and the pH means that the excitation intensity at a certain local position depends on a pH distribution along the path of the incident light. The DeLIF technique, which obtains the local excitation intensity from the fluorescence intensity of a non-active dye, makes the pH measurement simpler than the single-color LIF. This is a quite different character from the temperature measurement by LIF, in which only the quantum efficiency depends on the temperature.

Quinine is a common pH indicator. There are many other dyes useful for measuring pH near neutral conditions ($5 < \mathrm{pH} < 9$), however, quinine is quite useful and unique at approximately pH 3. Therefore, quinine was selected as a pH-dependent dye in the present paper. Another pH- and temperature-independent dye was searched by examining the absorption/emission spectra of many kinds of dyes and by referring to literature [3–5].

The absorption spectrum of quinine was investigated in detail at first. Buffer solution, composed of $KHC_8H_4O_4$ and NaOH, with an equivalent concentration of dye in a quartz glass cuvette with a 10mm path, was held in an aluminum holder to keep temperature constant and the spectrum was measured using a spectrograph. All spectra in the present paper were averaged for several measurements. Here, the addition of dye did not affect the pH of the solution, which was measured using an electro-pH-meter. The absorption spectra of quinine at different pH conditions are shown in Fig. 3 (294 K, 1.54×10^{-3} mol/l). The fluorescence of quinine was confirmed to depend on pH, and the shift of absorptivity occurred near pH 5. The desirable wavelength of the excitation light was from 345 to 365 nm. The vertical

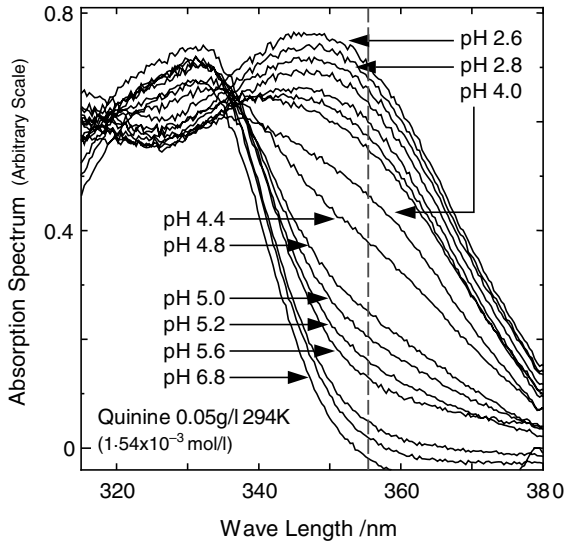

Fig. 3. Absorption spectra of quinine.

broken line shows the wavelength of the excitation light, 355 nm, in the present study. The emission spectrum of quinine, which has large peak between 400 and 570 nm, was also investigated.

Then, the absorption spectra of other dyes, which were expected to be independent of pH, were investigated. The pH-independent dye should not absorb strongly between 400 and 570 nm and should emit fluorescence at wavelengths over 580 nm. Absorbing the fluorescence emitted from quinine strongly would decrease the pH resolution, and it would affect also the fluorescence intensity of pH-independent dye though the fluorescence intensity of quinine was much smaller than the intensity of excitation light. Several kinds of common fluorescence dye, therefore, were not suitable for the pH-independent dye, e.g., Rhodamine(Rh) 6G, Rh 110, Rh 123 and Eosin Y. In addition, Rh6G showed an unstable property due to the quenching phenomenon. Sulforhodamine(SRh) showed relatively good characteristics, with an absorption wavelength peak at about 580 nm, as shown in Fig. 4 (294 K, 0.865×10^{-4} mol/l). The spectrum, the molar absorption, was independent of pH, i.e., also the emission spectrum would not depend on pH. SRh could be excited by a 355 nm wavelength due to its high quantum efficiency. Alternative dyes, which cost much higher, were available, but were not suitable for our bulk system. SRh was selected as the pH-independent dye.

As shown in Fig. 5, the emission spectra of a mixed dye solution (0.193×10^{-5} mol/l quinine + 0.865×10^{-6} mol/l SRh, 294 K) were investigated for different pH conditions with an excitation wavelength of 355 nm. The fluorescence intensity from quinine, less

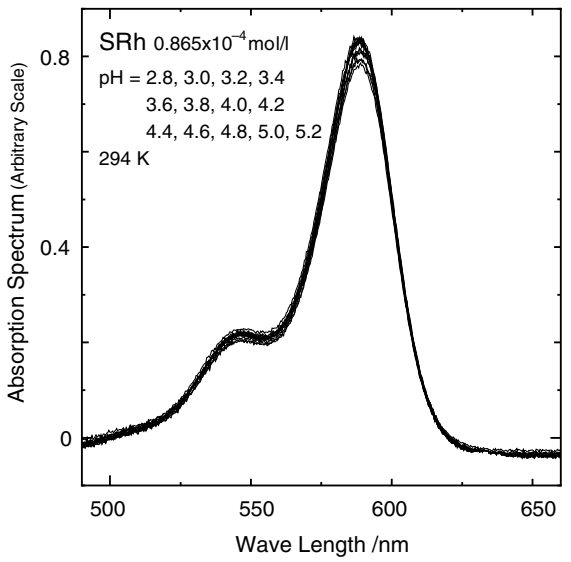

Fig. 4. Absorption spectra of sulforhodamine.

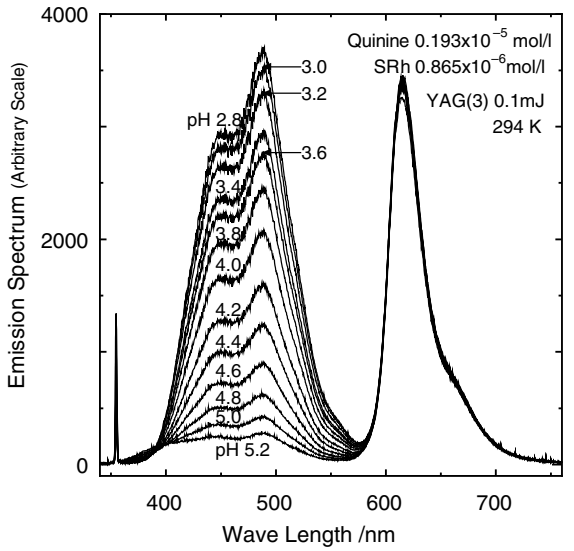

Fig. 5. Emission spectra of mixed dye solution.

than 570 nm, was affected by pH, but that from SRh, over 580 nm, was independent of pH, at pH between 5.2 and 2.8, in our experimental system. It was relatively easy to separate the fluorescence from each dye due to the large peak shift using a common dichroic beam splitter as shown in Fig. 1.

3. Experiments and results

3.1. Relationship between pH and fluorescence intensity ratio

As mentioned above, fluorescence dyes were selected using a spectrograph. Then, the relationship between intensity ratio and pH was investigated at atmospheric pressure, using our measurement system with the high-pressure vessel shown in Fig. 1. Fig. 6 shows examples of the relationship for different ratios of the dye concentration. Broken lines in Fig. 6 were calculated by the least square method for data with pH < 5.0. In Fig. 6, the buffer solution with the dyes was used for controlling pH, that is, the pH of solution was quite stable despite any impurities. For one concentration ratio, the relationship was also measured using H_2SO_4 solution and NaOH solution to examine the hysteresis of the relationship, as shown in Fig. 7. No hysteresis damping could be observed.

The calibration curve also depended on the location of the image [4], thus the relationship between pH and the ratio was obtained for each measurement point in the field of view. We calculated the calibration curve in each 8×8 pixel region. The intensity ratio at a certain pH required measurement by creating a uniform pH

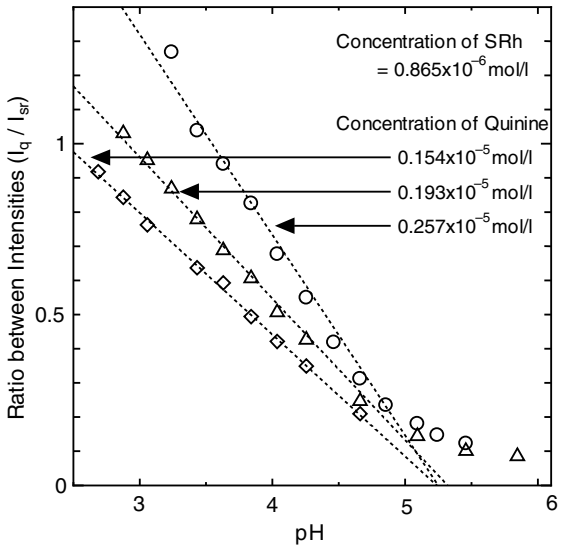

Fig. 6. Ratio between two cameras' output vs. pH (buffer solution).

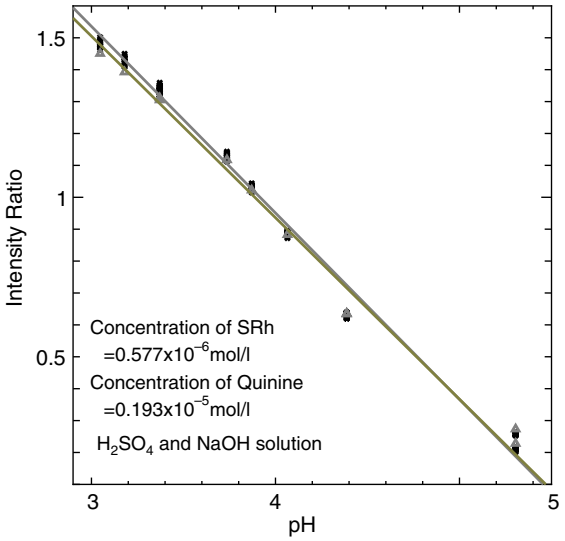

Fig. 7. Hysteresis of the ratio vs. pH for H_2SO_4 + NaOH solution.

field in the solution prior to each experiment, to fit a calibration curve with the pre-calibrated one. This process compensated for the fluctuation of the dye concentration ratios. Root mean square of the intensity ratio for 30 images, with uniform pH condition and with unstable excitation intensities of the pulse laser, was 0.001–0.002 of pH.

Here, the reference image was recorded at 0.1 MPa condition because authors couldn't get any other pH meter adaptable in the high pressure condition. It was assumed, therefore, that the fluorescence intensity itself was never affected by pressure and that the physical properties, i.e. the dissociation constants and the ion product of water, were correct.

3.2. Captured images

In order to demonstrate the applicability of our new system to pH measurement under high-pressure conditions, it was tried to measure the pH distribution around a dissolving CO_2 droplet at 9.81 MPa, 288 K. Fig. 8(a) and (b) show the visualized fluorescence intensity map (raw image data) of pH-dependent dye, and of pH-independent dye, respectively. Fig. 8(c) shows the map of processed intensity ratios, in the form of an 8 bit gray-scale image for convenience. Visualized images were captured approximately 1 min after CO_2 injection. No convection current driven by the temperature difference was observed, at least, before the CO_2 injection.

Fig. 8(a) shows a bright layer around the droplet, which represents the low pH region. The CO_2 droplet itself did not illuminate since there was no dye in it. The CO_2-dissolved water flowed downward due to its heavier density. The bright layer indicated that the gradient of pH and CO_2 concentration was very large near the interface. Due to reflection, refraction and absorption in the liquid CO_2 droplet, the intensity of the incident light at the left side of the droplet in Fig. 8(a) (the right side in Fig. 8(b)) became smaller.

Fig. 8(b) shows the map of the incident excitation intensity, including the influence of the reflection. In Fig. 8(b), it is easier to understand the position of the droplet's interface. The incident light is reflected and refracted at the apex of the droplet. A narrow dark ring-area just outside of the interface in Fig. 8(b), was due to less absorption by SRh as a result of much greater absorption by quinine. This effect was considered in the calibration curve. The bright region inside of the black ring seemed to be caused by reflection.

The distribution of the intensity ratio is shown in Fig. 8(c). The image coordinate in Fig. 8(c) was converted to match that in Fig. 8(b). The bright area shows the low pH area. The brightest region in Fig. 8(c) appeared near the interface between the drop-apex and the ambient solution. The influence of reflection and refraction seemed to be successfully removed, e.g., the refraction at the apex of drop shown in Figs. 8(a) and (b).

3.3. pH distribution around CO_2 droplet

Applying the local relationship between pH and the ratio of fluorescence intensities, the map of ratio shown in Fig. 8(c) could be converted into the pH distribution map. Fig. 9 is an example of a pH distribution map around the CO_2 droplet. The lowest pH value was 3.12. Fig. 9 shows that the pH gradient was very large

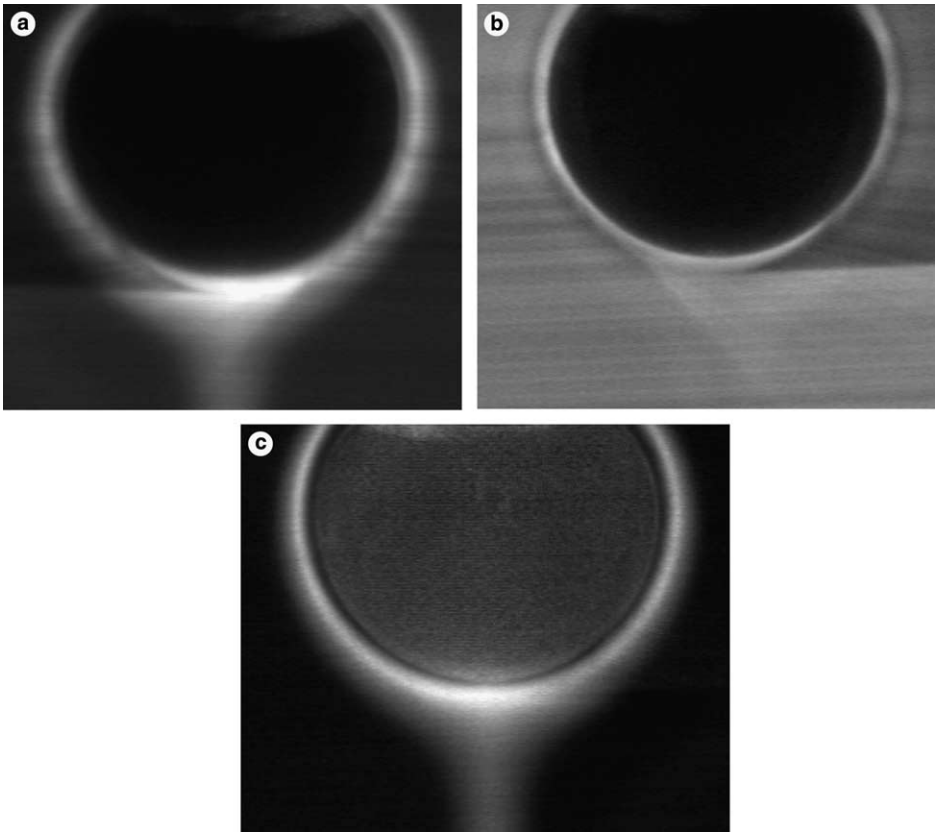

Fig. 8. Sample of a captured image pair and a processed image. (a) Intensity of pH dependent dye; (b) intensity of pH independent dye; (c) processed image.

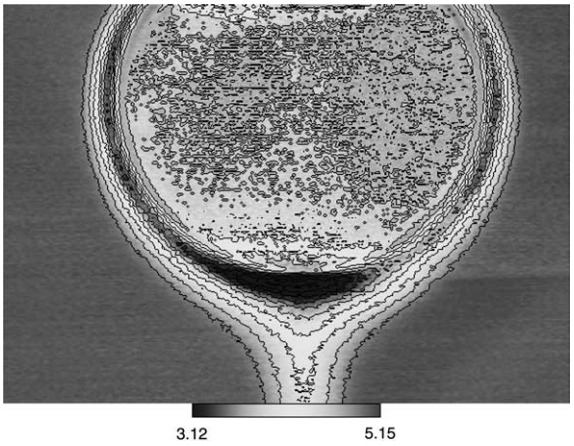

Fig. 9. Calculated pH distribution (288 K, 9.81 MPa).

near the interface. The thickness of the CO_2-enriched layer ($\approx CO_2$ concentration boundary layer) was approximately 220 μm in Fig. 9. The dissolved CO_2 diffused little beyond this layer and the CO_2-dissolved water flowed only downward. Thus, the pH distribution could be measured even in the high-pressure condition. This pH measurement method could be very useful for any other chemical reaction system.

Then, it was tried to estimate the CO_2 concentration distribution, which could be calculated from the pH distribution using the following equations, Eq. (3)–(9). The decrease of pH, the CO_2 dissolution into pure water, corresponds to these reactions. Here, the CO_2 concentration estimated from pH reflects the pH scale. The optical pH indicator directly shows the concentration of dissociating free hydrogen ions. In the present study, the ratio of fluorescence intensity was calibrated with a glass electrode pH-meter (KCl), i.e., the pH scale of pH_{NBS} ($\approx pH_a$) [6], as determined by the International Union of Pure and Applied Chemistry (IUPAC).

$$CO_2 + H_2O \Longleftrightarrow H_2CO_3 \tag{3}$$

$$H_2CO_3 \Longleftrightarrow H^+ + HCO_3^-$$
$$K_1 = ([H^+][HCO_3^-])/[H_2CO_3] \tag{4}$$

$$HCO_3^- \Longleftrightarrow H^+ + CO_3^{2-}$$
$$K_2 = ([H^+][CO_3^{2-}])/[HCO_3^-] \quad (5)$$

$$H_2O \Longleftrightarrow H^+ + OH^- \quad K_w = [H^+][OH^-] \quad (6)$$

$$A_t = [HCO_3^-] + 2[CO_3^{2-}] + [OH^-] = [H^+] \quad (7)$$

$$\sum CO_2 = [H_2CO_3] + [HCO_3^-] + [CO_3^{2-}] \quad (8)$$

$$\sum CO_2 = \left(\frac{[H^+]}{[H^+] + 2K_2}\right) \cdot \left(1 + \frac{K_2}{[H^+]} + \frac{[H^+]}{K_1}\right) \cdot \left([H^+] - \frac{K_w}{[H^+]}\right) \quad (9)$$

Here, $K_{i=1,2}$ are the dissociation constants for carbonic acid, CO_2 in pure water. K_w is the ion product of water. K_1, K_2 and K_w must be suitable for the pH_{NBS} scale. A_t is the total alkalinity. $\sum CO_2$ is the total carbon concentration. $K_{i=1,2}$ and K_w are dependent on the pressure and K_w is also a function of the temperature. The values of the $K_{i=1,2}$ and K_w at 9.81 MPa were obtained from references [6–8]. Saruhashi [7] introduced the $K_{i=1,2}$ as Eqs. (10) and (11), here, Eq. (10) was estimated using Saruhashi's data[7] with the least square method. Eq. (12) was also calculated using data from Marshall and Franck [8].

$$pK_1 = 3416.6675/T + 0.032902T - 14.9179 \quad (10)$$

$$pK_2 = 2902.39/T + 0.02379T - 6.4980 \quad (11)$$

$$K_{w_{(0.1\ MPa)}} = 3.7853T^3 \times 10^{-19} - 3.1197T^2 \times 10^{-16} + 8.5871T \times 10^{-14} - 7.8923 \times 10^{-12}$$
$$K_{w_{(p)}}/K_{w_{(0.1MPa)}} = 1.0006171 + 9.0589 \times 10^{-3}p + 4.4532 \times 10^{-5}p^2 \quad (12)$$

Applying the measured pH ($[H^+]$) and Eqs. (10)–(12) to Eq. (9), the distribution of CO_2 concentration could be calculated as shown in Fig. 10. The dissolution of CO_2 decreased pH to approximately 3.12 near the apex of the droplet. The highest CO_2 concentration was about 1.59 mol/l(≈0.0286 mol fraction). The CO_2 concentration just on the interface means the CO_2 solubility, while it was not observed clearly in Fig. 10 due to the relatively low spatial resolution. The highest value, however, was expected to be the solubility.

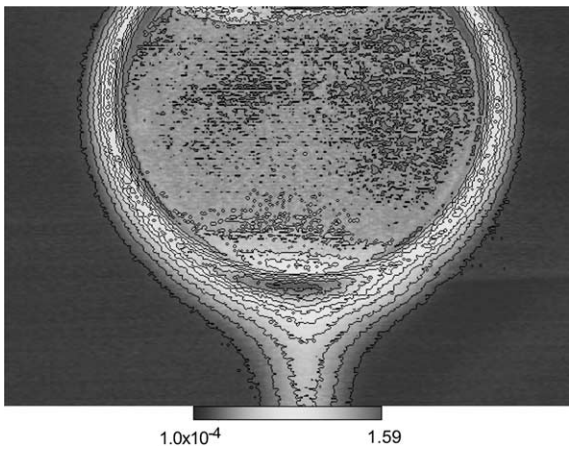

Fig. 10. Calculated CO_2 concentration (/mol l^{-1}) distribution.

On the other hand, Someya et al.[9] measured the CO_2 mole fraction at two phase equilibria, i.e., the solubility, under the same condition by a gas expanding method. The CO_2 solubility at 288 K and at 9.81 MPa measured by the conventional static method was about 0.0283 (±0.00015) of mole fraction.

These two measured values of solubility do not exactly coincide, however, they are close enough to conclude that the DeLIF method can be applied for estimating the solubility, not only for monitoring a sequestrated CO_2 behavior. The difference may be caused by the low spatial-and color-resolution of CCD cameras, and by an assumption in the present study, i.e., that the fluorescence intensity is not affected by the pressure. For confirming it, the relation between the fluorescence intensity and the pH should be calibrated at high pressure conditions, by using a new kind of 1-dimensional pH meter, which can be used at high pressure conditions.

Thus, the optical measurement method, DeLIF, is appropriate especially for studying the dynamic behavior in a high-pressure system. DeLIF is quite useful to investigate the varying pH distribution in the CO_2 solution at every moment. It can be also applied to measure the CO_2 solubility. There are some non-optical methods, however, they require long time and much information about non-target values. In contrast, because the fluorescence intensity is a function of pH, to estimate the CO_2 solubility by DeLIF method does not need so much time and information except for the ion product and the dissociation constants.

4. Conclusions

The pH distribution around a CO_2 droplet at the high-pressure condition was measured using the DeLIF technique with quinine and sulforhodamine. The characteristics of their spectra were examined against different pH conditions. This technique made it possible to measure the pH distribution and the CO_2 concentration distribution with good accuracy.

Acknowledgement

We gratefully acknowledge discussions with Dr. J. Sakakibara, Tsukuba University. The present study was supported by the Science and Technology Research Grant Program for Young Researchers with a Term

from the Ministry of Education, Culture, Sports, Science and Technology (MEXT) of Japan.

References

[1] C. Marchetti, On Geoengineering and the CO_2 problem, Clim. Change 1 (1977) 59–68.
[2] S. Someya, M. Nishio, B. Chen, H. Akiyama, K. Okamoto, Visualization of the dissolution behavior of a CO_2 droplet into seawater using LIF, J. Flow Visual. Image Proc. 6 (1999) 243–259.
[3] J. Coppeta, C. Rogers, Dual emission laser induced fluorescence for direct planar scalar behavior measurements, Exp. Fluids 25 (1998) 1–15.
[4] J. Sakakibara, R.J. Adrian, Whole field measurement of temperature in water using two-color laser induced fluorescence, Exp. Fluids 26 (1999) 7–15.
[5] J. Sakakibara, R.J. Adrian, Measurement of temperature field of a Rayleigh–Benard convection, Exp. Fluids 37-3 (2004) 331–340.
[6] E.Z. Rechard, W. Dieter, CO_2 in seawater: equilibrium, kinetics, isotopesElsevier Oceanography Series 65, Elsevier science B.V., Amsterdam, 2003, p. 55.
[7] K. Saruhashi, Tansan-gasu-to-tansan-busshitsu, in: S. Horibe (Ed.), Kaisui-no-kagaku, Tokai Univ. Press, Tokyo, 1970, pp. 3.3.2.242–3.3.2.268 (in Japanese).
[8] W.L. Marshall, E.U. Franck, Ion product of water substance 0-1000C 1-10000 bars new international formulation and its background, J. Phys. Chem. Ref. Data 10 (2) (1981) 295–304.
[9] S. Someya, S. Bando, B. Chen, Y. Song, M. Nishio, Measurement of the CO_2 solubility in pure water and the pressure effect on it in the presence of clathrate hydrate, Int. J. Heat Mass Trans.